

Hybrid Materials

International Edition: DOI: 10.1002/anie.201806862
German Edition: DOI: 10.1002/ange.201806862Rational Design of MOF/COF Hybrid Materials for Photocatalytic H₂ Evolution in the Presence of Sacrificial Electron DonorsFeng-Ming Zhang[†], Jing-Li Sheng[†], Zhao-Di Yang, Xiao-Jun Sun, Hong-Liang Tang, Meng Lu, Hong Dong, Feng-Cui Shen, Jiang Liu, and Ya-Qian Lan*

Abstract: Crystalline and porous covalent organic frameworks (COFs) and metal-organic frameworks (MOFs) materials have attracted enormous attention in the field of photocatalytic H₂ evolution due to their long-range order structures, large surface areas, outstanding visible light absorbance, and tunable band gaps. In this work, we successfully integrated two-dimensional (2D) COF with stable MOF. By covalently anchoring NH₂-UiO-66 onto the surface of TpPa-1-COF, a new type of MOF/COF hybrid materials with high surface area, porous framework, and high crystallinity was synthesized. The resulting hierarchical porous hybrid materials show efficient photocatalytic H₂ evolution under visible light irradiation. Especially, NH₂-UiO-66/TpPa-1-COF (4:6) exhibits the maximum photocatalytic H₂ evolution rate of 23.41 mmol g⁻¹ h⁻¹ (with the TOF of 402.36 h⁻¹), which is approximately 20 times higher than that of the parent TpPa-1-COF and the best performance photocatalyst for H₂ evolution among various MOF- and COF-based photocatalysts.

With increasing concern about the global problems of energy crisis and environmental pollution, finding sustainable and clean energy sources alternative to fossil fuels has become one of the most significant challenges for the human society.^[1] Light-driven water splitting into hydrogen is a very active field of energy research for the most promising strategies to obtain alternative energy sources.^[2] Therefore, enormous efforts have been devoted to develop efficient photocatalytic systems for hydrogen evolution via photoinduced water splitting.^[3] Covalent organic frameworks (COFs) and metal-organic frameworks (MOFs), as crystalline and porous materials assembled with pure organic molecules or and metal ions (metal clusters) by covalent or coordinated bonds, have been employed for various areas such as gas storage,^[4]

catalysis,^[5] and sensing.^[6] More recently, COFs have emerged as a new class of photoactive materials for light-induced H₂ evolution because of their long-range order structures, outstanding surface areas, and tunable band gaps.^[7] Besides, as constructed entirely from covalent bonds, COFs often show excellent chemical stabilities, especially in imine-linked and other nitrogen-containing COFs.^[8] Most of reported COFs until now are main 2D structures with intense interaction between the adjacent layers. The π - π stacking mediates electronic interactions between the layers, thus providing another possible pathway for charge carrier transport besides transfer within the covalent sheets.^[9] In addition, most COFs, especially Schiff-base COFs, usually exhibit orange to dark red color for the characteristic absorbance of groups and large conjugation system, and lead to a broader light harvesting in visible-light region and utilization.^[10] Until now, the reports about H₂ evolution with 2D COFs are still limited and hydrogen production rate as high as 1.9 mmol g⁻¹ h⁻¹ has been obtained.^[11] However, the hydrogen production rate is far from the expected and not as good as traditional semiconductors photocatalysts such as metal oxide and sulfide.^[12] One probably main reason that limits the H₂ evolution rate of COFs is the strong recombination of photogenerated electron-hole pairs.

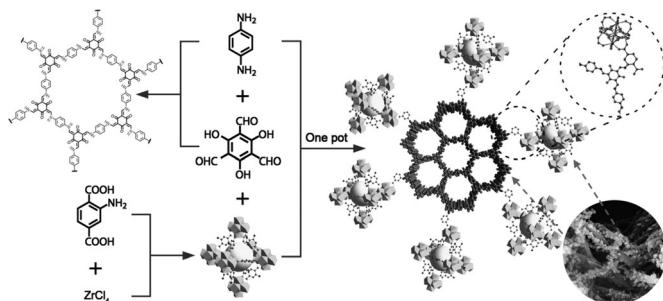
To improve the charge-carrier separation, an effective strategy is to develop proper semiconductor composites that make sure the opposite migration of electrons and holes by conduction-band (CB) and valence-band (VB) offsets.^[13] As the nature of crystalline organic porous polymers with well-defined pore structures, COFs allow molecular-level modification, surface engineering^[14] and serve as an outstanding host matrix to support metal nanoparticles or other species.^[15] Thus, some COF-supported Au, Pd, and CdS hybrid materials with improved catalytic activity have been prepared and reported.^[16] However, most of these researches mainly concentrated on the combination of two different species with weak interaction between them, while covalent bonds connection between parent components is very limited in the reported literatures. It can be predicted that covalent connection between host and guest species in composite is more beneficial to photogenerated electron transfer between them, and this assemble pattern can result in strong combination of different species.^[17] At the same time, it is also important to maintain the porosity of the resulting material when design and build a hybrid material to maximally allow the contact of reactant substrate with catalysts. The integration of MOF and COF that are two famous types of porous materials could inherent the high porosity of the parent species in the resulting hybrid materials.

[*] Dr. F.-M. Zhang,^[†] J.-L. Sheng,^[†] Prof. Z.-D. Yang, Prof. X.-J. Sun, H.-L. Tang, H. Dong
Key Laboratory of Green Chemical Engineering and Technology of College of Heilongjiang Province, College of Chemical and Environmental Engineering, Harbin University of Science and Technology No. 4, Linyuan Road, Harbin 150040 (China)
M. Lu, F.-C. Shen, Dr. J. Liu, Prof. Y.-Q. Lan
Jiangsu Collaborative Innovation Centre of Biomedical Functional Materials, Jiangsu Key Laboratory of New Power Batteries, School of Chemistry and Materials Science, Nanjing Normal University No. 1, Wenyuan Road, Nanjing, 210023 (China)
E-mail: yqlan@njnu.edu.cn

[†] These authors contributed equally to this work.

Supporting information and the ORCID identification number(s) for the author(s) of this article can be found under:
<https://doi.org/10.1002/anie.201806862>.

In this work, we design and construct a type of covalently integrated MOF/COF hybrid material exhibiting outstanding photocatalytic H_2 evolution rate. TpPa-1-COF was chosen to construct the composite given its typical structure of Schiff-base COFs. The resulting $\text{NH}_2\text{-UiO-66/TpPa-1-COF}$ composites were synthesized by introducing $\text{NH}_2\text{-UiO-66}$ into the reaction system of the synthesis of TpPa-1-COF (Scheme 1).



Scheme 1. Schematic illustration of the synthesis of $\text{NH}_2\text{-UiO-66/TpPa-1-COF}$ hybrid material.

The obtained $\text{NH}_2\text{-UiO-66/TpPa-1-COF}$ hybrid materials possess high surface area, porous framework, and high crystallinity. Thanks to the matching of band gaps between MOF and COF, the resulting series of composites exhibit effective visible-light-driven photocatalytic H_2 evolution with the maximum photocatalytic H_2 evolution efficiency of $23.41 \text{ mmol g}^{-1} \text{ h}^{-1}$ (with the TOF of 402.36 h^{-1}), which is approximately 20 times higher than that of the parent TpPa-1-COF and is the best performance photocatalyst for H_2 evolution among various MOF- and COF-based photocatalysts.

$\text{NH}_2\text{-UiO-66}$ was prepared by heating DMF solution containing ZrCl_4 and 2-aminoterephthalic acid ($\text{NH}_2\text{-BDC}$) ligand at 80°C with stirring. The structure of as-synthesized sample was confirmed by powder X-ray diffraction (PXRD) analysis and Fourier transform infrared (FT-IR) spectroscopy (Figure S1 and S2). Series of MOF/COF hybrid materials were prepared by adding different proportion of $\text{NH}_2\text{-UiO-66}$ nanoparticles into the synthetic reaction system of TpPa-1-COF with slightly extra 1,3,5-triformylphloroglucinol (Tp). The PXRD patterns of $\text{NH}_2\text{-UiO-66/TpPa-1-COF}$ hybrid materials exhibit intense peaks at 4.7° , corresponding to the reflection from the (100) plane of TpPa-1-COF (Figure 1a). All the peaks of $\text{NH}_2\text{-UiO-66/TpPa-1-COF}$ show good agreement with the corresponding simulated PXRD patterns of TpPa-1-COF and $\text{NH}_2\text{-UiO-66}$ demonstrating the formation of TpPa-1-COF and structural integrity of $\text{NH}_2\text{-UiO-66}$ in the resulting series of hybrid materials. With the increasing of the content of $\text{NH}_2\text{-UiO-66}$, the intensity of characteristic peaks from MOF apparently increases. Combined with their FT-IR spectra (Figure S3), it can be concluded that series of $\text{NH}_2\text{-UiO-66/TpPa-1-COF}$ hybrid materials have been successfully synthesized.

Thermogravimetric analyses (TGA) under air atmosphere reveals that TpPa-1-COF, $\text{NH}_2\text{-UiO-66}$ and series of $\text{NH}_2\text{-UiO-66/TpPa-1-COF}$ hybrid materials show thermal stability up to 400°C but with different residual weight at

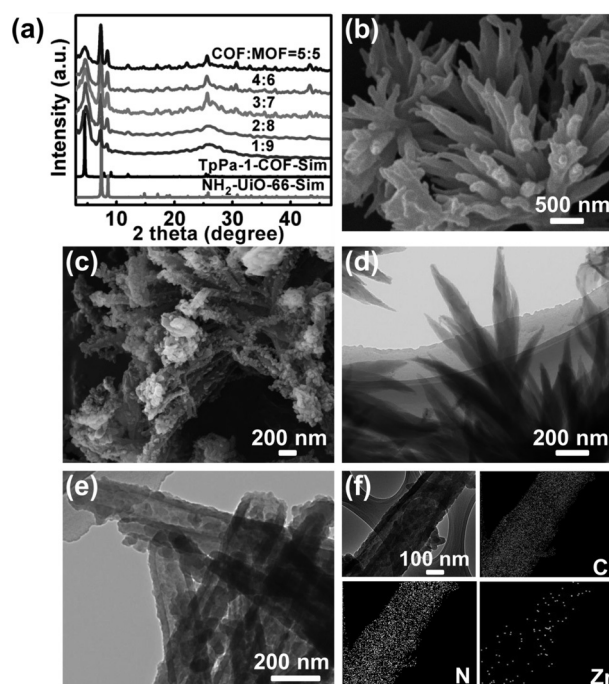


Figure 1. a) The PXRD patterns of $\text{NH}_2\text{-UiO-66/TpPa-1-COF}$ hybrid materials. b, c) SEM images of TpPa-1-COF and $\text{NH}_2\text{-UiO-66/TpPa-1-COF}$ (4:6). d, e) TEM images of TpPa-1-COF and $\text{NH}_2\text{-UiO-66/TpPa-1-COF}$ (4:6). f) HRTEM image and the corresponding elemental mappings of C, N and Zr for $\text{NH}_2\text{-UiO-66/TpPa-1-COF}$ (4:6).

800°C (Figure S4). From the results of TGA, the weight ratio of TpPa-1-COF and $\text{NH}_2\text{-UiO-66}$ in $\text{NH}_2\text{-UiO-66/TpPa-1-COF}$ (4:6) was estimated to be 40.5:59.5, comparable to the experimental value. The permanent porosities of as-synthesized samples were evaluated by N_2 absorption and desorption experiments at 77 K. All of the absorption isotherms exhibit type I isotherm according to the IUPAC classification (Figure S5). Bare $\text{NH}_2\text{-UiO-66}$ possesses the largest Brunauer–Emmett–Teller (BET) surface area in all of these synthesized materials with the value of $980 \text{ m}^2 \text{ g}^{-1}$. With the content of $\text{NH}_2\text{-UiO-66}$ increasing, the saturated uptakes and BET surface areas of resulting hybrid materials obviously increase. The value of BET for $\text{NH}_2\text{-UiO-66/TpPa-1-COF}$ (4:6) was calculated to be $669 \text{ m}^2 \text{ g}^{-1}$, which was much higher than its parent TpPa-1-COF ($490 \text{ m}^2 \text{ g}^{-1}$). The pore size distributions of as-synthesized samples (Figure S6), calculated on the basis of density functional theory (DFT), are comparable to the reported values.^[18]

The image of scanning electron microscopy (SEM) indicates that the as-synthesized $\text{NH}_2\text{-UiO-66}$ exhibits sheet morphology with particle size below 100 nm (Figure S7). Bare TpPa-1-COF shows a flowerlike morphology with the length of single branch stretching to several microns (Figure 1b), which is similar to that reported previously.^[19] The difference of morphology between TpPa-1-COF and $\text{NH}_2\text{-UiO-66/TpPa-1-COF}$ is that there are uniform distributed $\text{NH}_2\text{-UiO-66}$ particles attached on the surface of TpPa-1-COF (Figure 1c). The images of transmission electron microscopy (TEM) TpPa-1-COF and $\text{NH}_2\text{-UiO-66/TpPa-1-COF}$ further demonstrate that nanoparticles of $\text{NH}_2\text{-UiO-66}$ uniformly

distribute on the surface of TpPa-1-COF (Figure 1d-e). The result of high-resolution transmission electron microscopy (HRTEM) apparently shows the porous structure of COF in $\text{NH}_2\text{-UiO-66/TpPa-1-COF}$ (4:6) (Figure S8). The images of element mapping show that C, N, and Zr are densely distributed the entire frame (Figure 1f), which is consistent with aforementioned morphology of $\text{NH}_2\text{-UiO-66/TpPa-1-COF}$. The results of energy-dispersive X-ray spectroscopy (EDS) and Inductively coupled plasma optical-emission spectroscopy (ICP-OES) show that the average content of Zr is about 12.50 and 12.62 wt %, respectively, which are comparable to the calculated value 12.72 wt % (Figure S9).

UV/Vis diffuse reflectance spectra (DRS) measurements of the as-synthesized samples show that $\text{NH}_2\text{-UiO-66}$ exhibits a narrow optical absorbance with the edge at 440 nm, while the absorbance of TpPa-1-COF even cover the whole UV/Vis region with a broadly intense absorbance below 600 nm (Figure 2a). The $\text{NH}_2\text{-UiO-66/TpPa-1-COF}$ (4:6) hybrid

material well inherits the optical feature of TpPa-1-COF and exhibits the similar optical absorbance with it. The corresponding band gaps for $\text{NH}_2\text{-UiO-66}$ and TpPa-1-COF were calculated to be 2.88 and 2.02 eV, respectively. The results of Mott-Schottky measurements indicate that the flat band position (V_{fb}) of $\text{NH}_2\text{-UiO-66}$ and TpPa-1-COF is approximately -0.75 and -0.96 eV vs. the saturated calomel electrode (SCE), respectively (Figure 2b). Since it is generally believed that the bottom of the CB in many n-type semiconductors is more negative by about 0.10 V than the V_{fb} ,^[20] the CB of $\text{NH}_2\text{-UiO-66}$ and TpPa-1-COF was estimated to be -0.60 and -0.80 eV, respectively. Combined with the band gap energy, the VB positions of $\text{NH}_2\text{-UiO-66}$ and TpPa-1-COF are 2.28 and 1.22 eV vs. NHE, respectively, suggesting that $\text{NH}_2\text{-UiO-66/TpPa-1-COF}$ (4:6) hybrid material shows the type II heterojunction.^[21]

Encouraged by the above characterization results, H_2 evolution experiments have been conducted under an irradiation of 300 W Xe lamp with a cut-off filter of 420 nm. Sodium ascorbate (SA) was chosen as an optimized sacrificial agent to capture the photogenerated holes of the photocatalyst (Figure S10). The results of comparison experiments for different contents of Pt as cocatalyst demonstrated that 3 wt % Pt was the optimized content of cocatalyst (Figure S11). Under the above reaction conditions, TpPa-1-COF displays a photocatalytic H_2 evolution rate of $1.22 \text{ mmol g}^{-1} \text{ h}^{-1}$ (Figure 2c and S12). After coupled with $\text{NH}_2\text{-UiO-66}$, H_2 evolution rate of the series of $\text{NH}_2\text{-UiO-66/TpPa-1-COF}$ hybrid materials exhibit obvious increase tendency until the weight ratio of MOF:COF = 4:6. $\text{NH}_2\text{-UiO-66/TpPa-1-COF}$ (4:6) hybrid material shows the maximum photocatalytic activity of $23.41 \text{ mmol g}^{-1} \text{ h}^{-1}$ under visible light irradiation (with the TOF of 402.36 h^{-1} based on the amount of $\text{NH}_2\text{-UiO-66}$), which is approximately 20 times higher than the parent TpPa-1-COF and the best performance in various MOF- and COF-based photocatalysts (Table S1). When the content of $\text{NH}_2\text{-UiO-66}$ excess 40 wt % in the resulting hybrid materials, the photocatalytic H_2 evolution rate shows decrease tendency, which may be attributed to the block of light harvesting to COFs from $\text{NH}_2\text{-UiO-66}$ on the surface the hybrid material (Figure S13). For the purpose of evaluating the stable performance of $\text{NH}_2\text{-UiO-66/TpPa-1-COF}$ (4:6) hybrid material, we conducted photocatalytic H_2 evolution experiments for 480 h under the aforementioned condition. Notably, the $\text{NH}_2\text{-UiO-66/TpPa-1-COF}$ (4:6) hybrid material shows excellent photocatalytic stability in the reused 20 consecutive cycles in 480 h (Figure 2d). Besides, the PXRD patterns and morphology of $\text{NH}_2\text{-UiO-66/TpPa-1-COF}$ (4:6) hybrid material are no obvious change before and after photocatalytic reaction (Figure S14 and S15). These results further demonstrate the durable stability of $\text{NH}_2\text{-UiO-66/TpPa-1-COF}$ hybrid material in the photocatalytic reaction.

Electrochemical impedance spectroscopy (EIS) measurement was carried out to evaluate the internal resistances for the charge transfer process of the samples.^[22] $\text{NH}_2\text{-UiO-66/TpPa-1-COF}$ (4:6) displays a smaller semicircular diameter of Nyquist curves compared with TpPa-1-COF (Figure 3a), demonstrating a smaller interfacial charge-transfer resistance. The photocurrent density of $\text{NH}_2\text{-UiO-66/TpPa-1-COF}$ (4:6) hybrid material is about 3.5 times as high as that of TpPa-1-COF (Figure 3b), indicating that hybrid material contributes to make the photogenerated charges separate. The slight decrease of photocurrent in the initial time could be attributed to establishing equilibrium between electrolyte solution and ITO electrode coated by material layer upon irradiation.^[23] The enhanced charge-separation efficiency is further confirmed by photoluminescence (PL) emission spectra (Figure 3c), where the PL intensity of $\text{NH}_2\text{-UiO-66/TpPa-1-COF}$ (4:6) hybrid material is significantly quenched in comparison with that of the parent TpPa-1-COF. Besides, the surface photovoltage spectroscopy (SPS) response of $\text{NH}_2\text{-UiO-66/TpPa-1-COF}$ (4:6) hybrid material is evidently stronger than that of TpPa-1-COF (Figure 3d), suggesting that the separation of photogenerated charges efficiency of TpPa-1-COF is markedly improved by constructing the heterojunction.

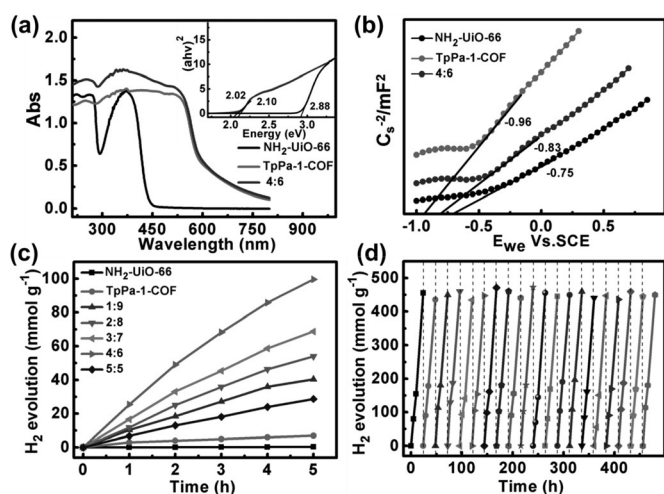


Figure 2. a) DRS and band-gap energies (inset) and b) Mott-Schottky plots for $\text{NH}_2\text{-UiO-66}$, TpPa-1-COF and $\text{NH}_2\text{-UiO-66/TpPa-1-COF}$ (4:6). c) The photocatalytic H_2 evolution activities. d) The photocatalytic stability of $\text{NH}_2\text{-UiO-66/TpPa-1-COF}$ (4:6).

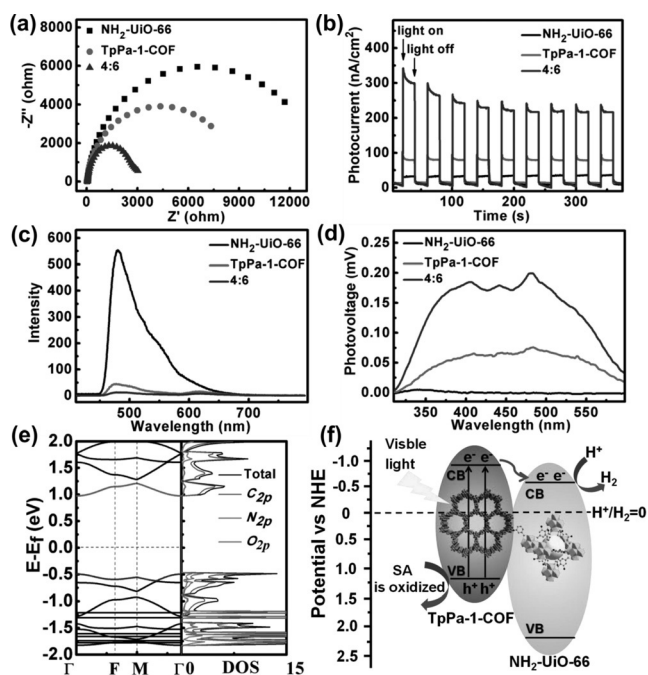


Figure 3. a) EIS Nyquist plots of $\text{NH}_2\text{-UiO-66}$, TpPa-1-COF and $\text{NH}_2\text{-UiO-66/TpPa-1-COF}$ (4:6) hybrid material. b) Transient photocurrents measurements. c) Photoluminescence spectra with the excitation wavelength of 350 nm. d) Surface photovoltage spectra. e) Band structures and density of states for monolayer TpPa-1-COF . f) Mechanism schematic of $\text{NH}_2\text{-UiO-66/TpPa-1-COF}$ (4:6) hybrid material.

We further probe the reason of the excellent H_2 evolution activity from the structure of $\text{NH}_2\text{-UiO-66/TpPa-1-COF}$ (4:6) by comparing the IR and solid-state ^{13}C CP/MAS NMR spectra of hybrid material and physical mixing sample. In the IR spectrum of hybrid material, typical peak of C=N group can be observed at 1622 cm^{-1} formed by Tp and $\text{NH}_2\text{-BDC}$ ligand of MOF (Figure S16). The ^{13}C CP/MAS NMR spectra of physical mixing just simply contain both the peaks of MOF and COF, even without change (Figure S17). However, the signals of hybrid are apparently different from that of physical mixing sample, especially the peaks of carbon atoms from the ligand of MOF in hybrid material have obvious shift for the structural change of ligand. Besides, differently from physical mixing sample, the typical signal of carbon from C=N group can be observed at 177.3 ppm in the ^{13}C CP/MAS NMR spectrum of hybrid material. These results demonstrate the covalence between MOF and COF in the hybrid material. To confirm the prominent role of covalent connection in hybrid materials, we prepared UiO-66/TpPa-1-COF (4:6) composite without probable covalent connection between these two species and physical mixing material of $\text{NH}_2\text{-UiO-66}$ and TpPa-1-COF (4:6) through grinding under room temperature. The SEM images of the UiO-66/TpPa-1-COF (4:6) show that the as-synthesized UiO-66 could not homogeneously grow on the surface of the TpPa-1-COF and just exist independently (Figure S18). This demonstrates that -NH_2 groups in MOF is essential to obtain the hybrid material, which is similar to recently reported $\text{NH}_2\text{-MOF}$ -based hybrid material modified with COF shell.^[24] Moreover, the photocatalytic activity of $\text{NH}_2\text{-UiO-66/TpPa-1-COF}$ (4:6)

hybrid material is approximately 5 times and 30 times higher than that of UiO-66/TpPa-1-COF (4:6) and physical mixing material (4:6), respectively (Figure S19). At the same time, compared with the UiO-66/TpPa-1-COF (4:6) and the physical mixing (4:6), $\text{NH}_2\text{-UiO-66/TpPa-1-COF}$ (4:6) hybrid material exhibits the smallest semicircular diameter of Nyquist curves, the highest photocurrent density, lowest PL intensity and highest SPS response (Figure S20–23). All of these results demonstrate the exit of covalent bond between two species in $\text{NH}_2\text{-UiO-66/TpPa-1-COF}$ and its essential function to improving photogenerated electron transfer in the heterojunction.

We further conducted DFT calculation for the band gap of TpPa-1-COF (in Supporting Information), and the results indicate that TpPa-1-COF monolayer is a directly band gap (1.5 eV) semiconductor at Γ point (Figure 3e). The conduction band potential is -1.2 eV by converting to NHE at pH 7, which is slightly higher than the value of experimental data for the applying standard DFT method.^[25] The results of TEM and Pt mapping for the hybrid material after Pt loading show that Pt nanoparticles mainly distributed on MOF (Figure S24) and thus the mechanism for the catalytic system can be proposed as Figure 3f. In the $\text{NH}_2\text{-UiO-66/TpPa-1-COF}$, the component of TpPa-1-COF possesses excellent light absorbance ability and acts as a light-harvest role upon visible light irradiation. Then, photogenerated electrons of TpPa-1-COF migrate from VB to CB, which would further fleetly transfer to the CB of $\text{NH}_2\text{-UiO-66}$ through covalent connecting junction to make sure the opposite migration of photogenerated electrons and holes. The successfully separated electrons in the CB of $\text{NH}_2\text{-UiO-66}$ conduct the H^+ reduction under the Pt co-catalyst, and holes leaved in the VB of TpPa-1-COF are captured by SA.

In summary, we designed and synthesized a series of MOF/COF hybrid materials with the connection of covalent bonds between two species for photocatalytic H_2 evolution. The resulting $\text{NH}_2\text{-UiO-66/TpPa-1-COF}$ (4:6) hybrid material shows excellent photocatalytic H_2 evolution rate of $23.41\text{ mmol g}^{-1}\text{ h}^{-1}$ ($\text{TOF} = 402.36\text{ h}^{-1}$), which is approximately 20 times higher than that of the parent TpPa-1-COF and is the best performance photocatalyst for H_2 evolution among various MOF- and COF-based photocatalysts. The results of experiments and DFT calculation demonstrated that effective viable-light absorption of TpPa-1-COF , well-matching band gaps between $\text{NH}_2\text{-UiO-66}$ and TpPa-1-COF , and the efficient charge separation across the covalent heterojunction interface in the hybrid materials greatly contributed to the ultra-high H_2 evolution rate of $\text{NH}_2\text{-UiO-66/TpPa-1-COF}$ hybrid materials. This design strategy in this study opens up a new way for the construction of efficient MOF/COF hybrid photocatalysts for efficient hydrogen evolution.

Acknowledgements

This work was financially supported by NSFC (No. 21501036, 21676066, 21622104 and 21471080) and the special fund for scientific and technological innovation talents of Harbin

Science and Technology Bureau (No. 2017RAQXJ101 and 2017RAQXJ057), Priority Academic Program Development of Jiangsu Higher Education Institutions and the Foundation of Jiangsu Collaborative Innovation Center of Biomedical Functional Materials.

Conflict of interest

The authors declare no conflict of interest.

Keywords: covalent organic frameworks · hybrid materials · metal-organic frameworks · photocatalytic hydrogen evolution

How to cite: *Angew. Chem. Int. Ed.* **2018**, 57, 12106–12110
Angew. Chem. **2018**, 130, 12282–12286

- [1] a) S. Y. Ding, W. Wang, *Chem. Soc. Rev.* **2013**, 42, 548–568; b) H. Furukawa, O. M. Yaghi, *J. Am. Chem. Soc.* **2009**, 131, 8875–8883; c) F. Xu, H. Xu, X. Chen, D. C. Wu, Y. Wu, H. Liu, C. Gu, R. W. Fu, D. L. Jiang, *Angew. Chem. Int. Ed.* **2015**, 54, 6814–6818; *Angew. Chem.* **2015**, 127, 6918–6922; d) F. Beuerle, B. Gole, *Angew. Chem. Int. Ed.* **2018**, 57, 4850–4878; *Angew. Chem.* **2018**, 130, 4942–4972.
- [2] a) Y. J. Yuan, Z. T. Yu, D. Q. Chen, Z. G. Zou, *Chem. Soc. Rev.* **2017**, 46, 603–631; b) K. Christopher, R. Dimitrios, *Energy Environ. Sci.* **2012**, 5, 6640–6651; c) A. J. Esswein, D. G. Nocera, *Chem. Rev.* **2007**, 107, 4022–4047; d) J. H. Kou, C. H. Lu, J. Wang, Y. K. Chen, Z. Z. Xu, R. S. Varma, *Chem. Rev.* **2017**, 117, 1445–1514.
- [3] a) G. C. Xie, K. Zhang, B. D. Guo, Q. Liu, L. Fang, J. R. Gong, *Adv. Mater.* **2013**, 25, 3820–3839; b) X. B. Chen, S. H. Shen, L. J. Guo, S. S. Mao, *Chem. Rev.* **2010**, 110, 6503–6570; c) H. Tong, S. X. Ouyang, Y. P. Bi, N. Umezawa, M. Oshikiri, J. H. Ye, *Adv. Mater.* **2012**, 24, 229–251; d) M. F. Kuehnle, E. Reisner, *Angew. Chem. Int. Ed.* **2018**, 57, 3290–3296; *Angew. Chem.* **2018**, 130, 3346–3353; e) Q. Xiang, B. Cheng, J. Yu, *Angew. Chem. Int. Ed.* **2015**, 54, 11350–11366; *Angew. Chem.* **2015**, 127, 11508–11524.
- [4] a) W. Xia, C. Qu, Z. B. Liang, B. T. Zhao, S. G. Dai, B. Qiu, Y. Jiao, Q. B. Zhang, X. Y. Huang, W. H. Guo, D. Dang, R. Q. Zou, D. G. Xia, Q. Xu, M. L. Liu, *Nano Lett.* **2017**, 17, 2788–2795; b) S. T. Meek, J. A. Greathouse, M. D. Allendorf, *Adv. Mater.* **2011**, 23, 249–267.
- [5] a) W. Wang, X. M. Xu, W. Zhou, Z. P. Shao, *Adv. Sci.* **2017**, 4, 1600371; b) X. Han, Q. C. Xia, J. J. Huang, Y. Liu, C. X. Tan, Y. Cui, *J. Am. Chem. Soc.* **2017**, 139, 8693–8697; c) H. Li, Q. Y. Pan, Y. C. Ma, X. Y. Guan, M. Xue, Q. R. Fang, Y. S. Yan, V. Valtchev, S. L. Qiu, *J. Am. Chem. Soc.* **2016**, 138, 14783–14788.
- [6] a) J. L. Segura, M. J. Mancheno, F. Zamora, *Chem. Soc. Rev.* **2016**, 45, 5635–5671; b) P. J. Waller, S. J. Lyle, T. M. O. Popp, C. S. Diercks, J. A. Reimer, O. M. Yaghi, *J. Am. Chem. Soc.* **2016**, 138, 15519–15522.
- [7] a) Y. Zhao, *Chem. Mater.* **2016**, 28, 8079–8081; b) H. Xu, J. Gao, D. L. Jiang, *Nat. Chem.* **2015**, 7, 905–912.
- [8] a) B. P. Biswal, S. Chandra, S. Kandambeth, B. Lukose, T. Heine, R. Banerjee, *J. Am. Chem. Soc.* **2013**, 135, 5328–5331; b) S. Dalapati, S. B. Jin, J. Gao, Y. H. Xu, A. Nagai, D. L. Jiang, *J. Am. Chem. Soc.* **2013**, 135, 17310–17313; c) G. Das, B. P. Biswal, S. Kandambeth, V. Venkatesh, G. Kaur, M. Addicoat, T. Heine, S. Verma, R. Banerjee, *Chem. Sci.* **2015**, 6, 3931–3939.
- [9] a) T. Sick, A. G. Hufnagel, J. Kampmann, I. Kondofersky, M. Calik, J. M. Rotter, A. M. Evans, M. Dobliger, S. Herbert, K. Peters, D. Boehm, P. Knochel, D. D. Medina, D. Fattakhova-Rohlfing, T. Bein, *J. Am. Chem. Soc.* **2018**, 140, 2085–2092; b) T. Banerjee, F. Haase, G. Savasci, K. Gottschling, C. Ochsenfeld, B. V. Lotsch, *J. Am. Chem. Soc.* **2017**, 139, 16228–16234.
- [10] S. Chandra, S. Kandambeth, B. P. Biswal, B. Lukose, S. M. Kunjir, M. Chaudhary, R. Babarao, T. Heine, R. Banerjee, *J. Am. Chem. Soc.* **2013**, 135, 17853–17861.
- [11] T. Banerjee, K. Gottschling, G. Savasci, C. Ochsenfeld, B. V. Lotsch, *ACS Energy Lett.* **2018**, 3, 400–409.
- [12] a) K. Zhang, L. J. Guo, *Catal. Sci. Technol.* **2013**, 3, 1672–1690; b) A. Kudo, Y. Miseki, *Chem. Soc. Rev.* **2009**, 38, 253–278; c) V. Artero, M. Chavarot-Kerlidou, M. Fontecave, *Angew. Chem. Int. Ed.* **2011**, 50, 7238–7266; *Angew. Chem.* **2011**, 123, 7376–7405.
- [13] a) R. Marschall, *Adv. Funct. Mater.* **2014**, 24, 2421–2440; b) M. Calik, F. Auras, L. M. Salonen, K. Bader, I. Grill, M. Handloser, D. D. Medina, M. Dogru, F. Lobermann, D. Trauner, A. Hartschuh, T. Bein, *J. Am. Chem. Soc.* **2014**, 136, 17802–17807.
- [14] a) M. Calik, T. Sick, M. Dogru, M. Dobliger, S. Datz, H. Budde, A. Hartschuh, F. Auras, T. Bein, *J. Am. Chem. Soc.* **2016**, 138, 1234–1239; b) X. Chen, M. Addicoat, E. Q. Jin, L. P. Zhai, H. Xu, N. Huang, Z. Q. Guo, L. L. Liu, S. Irle, D. L. Jiang, *J. Am. Chem. Soc.* **2015**, 137, 3241–3247; c) S. Dalapati, M. Addicoat, S. B. Jin, T. Sakurai, J. Gao, H. Xu, S. Irle, S. Seki, D. L. Jiang, *Nat. Commun.* **2015**, 6, 7786.
- [15] F. Auras, L. Ascherl, A. H. Haldmioun, J. T. Margraf, F. C. Hanusch, S. Reuter, D. Bessinger, M. Dobliger, C. Hettstedt, K. Karaghiosoff, S. Herbert, P. Knochel, T. Clark, T. Bein, *J. Am. Chem. Soc.* **2016**, 138, 16703–16710.
- [16] a) X. F. Shi, Y. J. Yao, Y. L. Xu, K. Liu, G. S. Zhu, L. F. Chi, G. Lu, *ACS Appl. Mater. Interfaces* **2017**, 9, 7481–7488; b) R. S. B. Gonçalves, A. B. V. de Oliveira, H. C. Sindra, B. S. Archanjo, M. E. Mendoza, L. S. A. Carneiro, C. D. Buarque, P. M. Esteves, *ChemCatChem* **2016**, 8, 743–750.
- [17] a) M. Schreier, J. S. Luo, P. Gao, T. Moehl, M. T. Mayer, M. Gratzel, *J. Am. Chem. Soc.* **2016**, 138, 1938–1946; b) R. Göstl, S. Hecht, *Angew. Chem. Int. Ed.* **2014**, 53, 8784–8787; *Angew. Chem.* **2014**, 126, 8929–8932; c) C. L. Anfuso, R. C. Snoeberger, A. M. Ricks, W. M. Liu, D. Q. Xiao, V. S. Batista, T. Q. Lian, *J. Am. Chem. Soc.* **2011**, 133, 6922–6925.
- [18] M. J. Katz, Z. J. Brown, Y. J. Colon, P. W. Siu, K. A. Scheidt, R. Q. Snurr, J. T. Hupp, O. K. Farha, *Chem. Commun.* **2013**, 49, 9449–9451.
- [19] S. Kandambeth, A. Mallick, B. Lukose, M. V. Mane, T. Heine, R. Banerjee, *J. Am. Chem. Soc.* **2012**, 134, 19524–19527.
- [20] a) J. Wang, Y. Yu, L. Zhang, *Appl. Catal. B* **2013**, 136–137, 112–121; b) J. Zhang, X. Chen, K. Takanabe, K. Maeda, K. Domen, J. Epping, X. Fu, M. Antonietti, X. Wang, *Angew. Chem.* **2010**, 122, 451–454; c) A. Ishikawa, T. Takata, J. N. Kondo, M. Hara, H. Kobayashi, K. Domen, *J. Am. Chem. Soc.* **2002**, 124, 13547–13553.
- [21] M. Reza Gholipour, C. T. Dinh, F. Beland, T. O. Do, *Nanoscale* **2015**, 7, 8187–8208.
- [22] S. Banerjee, S. K. Mohapatra, P. P. Das, M. Misra, *Chem. Mater.* **2008**, 20, 6784–6791.
- [23] a) N. Iqbal, I. Khan, Z. H. Yamani, A. Ourashi, *Sci. Rep.* **2016**, 6, 32319; b) D. P. Kumar, S. Hong, D. A. Reddy, T. K. Kim, *Appl. Catal. B* **2017**, 212, 7–14.
- [24] Y. W. Peng, M. T. Zhao, B. Chen, Z. C. Zhang, Y. Huang, F. N. Dai, Z. C. Lai, X. Y. Cui, C. L. Tan, H. Zhang, *Adv. Mater.* **2018**, 30, 1705454.
- [25] H. J. Zhang, X. Q. Zuo, H. B. Tang, G. Li, Z. Zhou, *Phys. Chem. Chem. Phys.* **2015**, 17, 6280–6288.

Manuscript received: June 14, 2018

Accepted manuscript online: July 18, 2018

Version of record online: August 7, 2018